Soft Matter

Bilayer Aggregate Microstructure Determines Viscoelasticity of Lung Surfactant Suspensions

Journal:	*Soft Matter*
Manuscript ID	SM-ART-03-2021-000337.R1
Article Type:	Paper
Date Submitted by the Author:	20-Apr-2021
Complete List of Authors:	Ciutara, Clara; University of Minnesota, Chemical Engineering and Materials Science Zasadzinski, Joseph; University of Minnesota, Chemical Engineering and Materials Science

ARTICLE

Bilayer Aggregate Microstructure Determines Viscoelasticity of Lung Surfactant Suspensions

Clara O. Ciutara and Joseph A. Zasadzinski

Received 00th January 20xx,
Accepted 00th January 20xx

DOI: 10.1039/x0xx00000x

Neonatal respiratory distress syndrome (NRDS) is treated by intratracheal delivery of suspensions of animal-derived lung surfactant in saline. Lung surfactants are extracted via organic solvents from animal lung lavage, followed by solvent removal and surfactant re-hydration to form multi-bilayer particles suspended in saline. Following intra-tracheal administration, the surfactant suspension spreads throughout the lungs by surface tension gradient induced flow; the spreading rate is limited by suspension viscoelasticity. Here we examine the rheology of three clinical lung surfactant suspensions: Survanta (bovine lung), Curosurf (porcine lung), and Infasurf (calf lung). These surfactants have widely different rheological properties that depend on the lipid composition and bilayer organization. The steady shear viscosity is related to the bilayer particle volume fraction as for a suspension of hard spheres, but the lipid volume fraction is not simply related to the mass loading. Optical and electron microscopy and small angle X-ray scattering show that the viscosity variation is due to the temperature and composition dependent bilayer aggregate shapes and internal particle organization. Survanta forms crystalline bilayers at 37 °C, resulting in high aspect ratio asymmetric particles. Infasurf forms aggregates of unilamellar vesicles containing water pockets, while Curosurf forms onion-like multi-layered liposomes. While the mass loading of the three clinical surfactants is different, the different bilayer organization causes the particle volume fractions to be similar. Adding polyethylene glycol dehydrates and partially flocculates the bilayer aggregates in all suspensions, leading to smaller particle volume fractions and a reduced suspension viscosity even though the solvent viscosity increases almost six-fold.

1 Introduction

The interface between the epithelial lining fluid and air in lung alveoli is lined with lung surfactant (LS), a mixture of lipids and proteins that facilitates breathing by reducing the air-water interfacial tension, and thus the energy required to breathe [4-6]. A lack of functional surfactant is associated with two pathological conditions: Neonatal Respiratory Distress Syndrome (NRDS) and Acute Respiratory Distress Syndrome (ARDS). NRDS occurs in premature infants who are born prior to complete development of their lung surfactant system [7]. NRDS is successfully treated with replacement surfactants derived from animal sources [8-9]. ARDS is a more complex condition in adults and children and is a complication of lung trauma or disease, including COVID-19 infections. The inflammatory response to trauma or disease can lead to surfactant inactivation, which in turn can decrease lung compliance (pressure-volume response in the lung), promote atelectasis (alveoli filling with fluid) and other breathing issues which are typical symptoms of both NRDS and ARDS.

In the United States, the three clinically approved replacement lung surfactants are Survanta (minced bovine lung extract), Infasurf (calf lung lavage extract), and Curosurf (minced porcine lung extract). Although replacement surfactant therapy has been quite successful in treating NRDS, the composition, bilayer and monolayer properties of these three surfactants varies widely [9-11]. In addition, as these surfactants are animal-sourced, all clinical surfactants suffers somewhat from batch-to-batch variability and potential viral or prion contamination. Animal-derived surfactants have not been effective in treating ARDS; in fact, there are no generally accepted treatments or mechanistic understanding of the breathing instabilities associated with ARDS [12].

The composition of replacement LS are extrapolated from both bronchoalveolar lavage and pharyngeal aspirates of animals and humans, which were presumed to closely represent the composition of *in vivo* lung surfactant. By weight, extracted lung surfactant consists of 85% glycerol-phospholipids and 10% lung-specific proteins [11]. The remaining fractions are cholesterol and other neutral lipids such as triglycerides [13].

[a] *Department of Chemical Engineering and Materials Science, University of Minnesota, Minneapolis, Minnesota 55455*

† Footnotes relating to the title and/or authors should appear here.
Electronic Supplementary Information (ESI) available: [details of any supplementary information available should be included here]. See DOI: 10.1039/x0xx00000x

The dominant lipid (50% or more by weight) in all three clinical formulations is dipalmitoylphosphatidylcholine (DPPC), a di-saturated, zwitterionic, bilayer-forming lipid. In excess water or saline, pure DPPC bilayers undergo a transition at 37°C from the tilted hexagonally packed crystalline $L_{\beta'}$ phase to the less ordered, but rippled $P_{\beta'}$ phase. At 41°C, the crystalline bilayers melt to form the fluid L_{α} phase [14]. As most warm-blooded animals have body temperatures of 36 – 40°C, DPPC bilayers in LS are likely to be in the ordered $L_{\beta'}$ or $P_{\beta'}$ phases.

The bulk of the remaining lipid fraction of LS consists of unsaturated phosphatidylcholines (25-40% by weight), along with smaller fractions of anionic lipids such as phosphatidylglycerol [9]. Unsaturated lipids have much lower crystal to liquid transition temperatures than DPPC. For example, the single double bond in palmitoyloleoylphosphatidylcholine lowers the solid to fluid transition temperature to -2 °C. Mixtures of saturated and unsaturated lipids can phase separate within bilayers or monolayers to form coexisting liquid and solid phases [15].

In addition to the lipids, four lung surfactant specific proteins make up ~10 wt% of native surfactant. Two hydrophobic proteins, SP-B and SP-C are present at 1 - 2 wt% in replacement surfactants. The hydrophilic proteins SP-A and SP-D are not soluble in the organic solvents used to extract lung surfactant from lung lavage and are not present in replacement lung surfactants [9]. SP-A and SP-D are generally believed to enhance lung immunity and are part of the innate immune system in the lung.

The differences in lipid composition between the clinical lung surfactants likely play a major role in the differences in their suspension properties. Both Survanta and Curosurf remove any cholesterol from their formulations, Infasurf retains 5-8 wt% cholesterol (10-15 mol:mol% relative to the phospholipids) [9-10]. Cholesterol is ubiquitous in cell membranes and inevitably appears in the lavage material extracted from animal lungs prior to purification. It is still an open question if cholesterol is present in native human lung surfactant or what its role may be [13, 16]. Even small mole fractions of cholesterol decrease the ordering of DPPC at physiological temperatures. At sufficiently high cholesterol concentrations, the DPPC lattice is disrupted, and the mixture forms two immiscible liquid phases in both monolayers and bilayers. The cholesterol-rich phase is known as the liquid disordered (L_O) phase, and the cholesterol-poor phase is the liquid disordered phase (L_D) [17-18]. Both L_O and L_D phases are fluid at room temperature and above.

In addition to the extracted lipids, between 6-14 wt% saturated palmitic acid (PA) is added to Survanta [9-10]. PA co-crystallizes with DPPC, which increases the solid to fluid melting temperature in bilayers to 50-60°C for the mole ratios of DPPC:PA in Survanta [14, 19]. Hence, in Survanta, and to a lesser extent Curosurf and Infasurf, multiple solid and fluid phases can coexist in each bilayer at physiological temperature. The effects of these components on the bilayer aggregates in the clinical suspensions is not well understood nor is how the phase behaviour of the bilayers in these aggregates might influence the suspension viscosity.

DPPC, and the other saturated and unsaturated phosphatidylcholines, phosphatidylglycerols, and phosphatidylserines in LS self-assemble into lipid bilayers in saline. In the lungs, LS bilayers are further organized into "multilamellar bodies" that are extruded from the type II pneumocyte cells that line the alveoli into the alveolar line fluid [20-21]. These multilamellar bodies resemble multilamellar liposomes that form spontaneously on hydration of phospholipids [3]. On contact with the air-water interface in the lung, the multilamellar bodies transform into monolayers that spread to cover the alveolar interface. Previous optical microscopy and freeze-fracture transmission electron microscopy (FFTEM) results [3, 22-23] show that the bilayer aggregates of the three clinical surfactants are polydisperse and each has a unique internal structure and ordering, with aggregate sizes varying from 100 nm−10 μm, although the lipid bilayers are organized differently in the different surfactants.

For NRDS treatment, the surfactant suspension is instilled via an intratracheal tube and must rapidly flow through the multitude of airway bifurcations, and upon reaching the lung periphery, swiftly spread to cover the alveolar air-water interface as monolayers. Gravity is typically not the main driving force for such flows at the 1-100 μm length scales in the lung alveoli epithelial lining fluids; rather surface tension gradients drive such flows from areas of low surface tension to higher surface tension via Marangoni flow [24]. But whatever the driving force, the suspension viscoelasticity resists the flow. If the suspension has a yield stress or substantial elasticity, flow can be completely arrested. Rapid and complete spreading is also essential for drug delivery via surfactant suspensions to treat other bronchoalveolar diseases in preterm infants. Lung surfactants are well tolerated drug carriers as they are physiologically compatible to the airway and promote spreading of the drug to the distal portions of the lung [24-25].

While clinical lung surfactants have shown good efficacy in treating NRDS, they have been less successful in treating ARDS. One factor in LS inhibition in ARDS is the competition for the air-water interface by serum proteins and lysolipids resulting from lung inflammation processes [15]. These contaminants occupy the alveolar interface and reduce the driving force for adsorption of the lung surfactant aggregates to the air-water interface [15]. Previous studies have shown that the addition of polyethylene glycol (PEG), hyaluronan, dextran and other non-adsorbing hydrophilic polymers to the LS suspension induces a depletion attraction that causes the surfactant aggregates to adsorb more rapidly to air-water interfaces as well as flocculating in the suspension [3, 15, 26-32]. This effect has been shown to enhance oxygenation in animal models of ARDS and meconium aspiration syndrome [26-27, 29-33]. However, the effects on the suspension rheology of adding PEG to lung surfactants are unknown.

In practice, Survanta takes longer to restore breathing in NRDS patients compared to Curosurf and Infasurf, although there is little correlation between this initial lag time and long term complications or survival [34]. The Grotberg group has studied the flow of lung surfactant mixtures through airway-like bifurcations using microfluidic channels and theoretical modelling [35-37]. Their work is primarily concerned with the effects of local environment and geometry on the flow profile; the effects of different LS compositions on the flow properties of surfactant suspensions have not been examined.

Here, we investigated the bulk rheology of the three commonly used clinical surfactant suspensions. We find that the differences in lung surfactant composition dictate the structure of the bilayer aggregates in suspension, which in turn, dictate the rheological properties of the suspensions. At low shear rates, all three clinical surfactants are soft viscoelastic solids, with the elastic modulus greater than the loss modulus. The rigid, high aspect ratio aggregates formed by Survanta have a significant apparent yield stress at physiological temperature, while the spherical Curosurf and Infasurf have a smaller apparent yield stress. Increasing the temperature of Survanta above the bilayer solid-liquid transition lowers the suspension viscosity to that of Curosurf and Survanta as the Survanta aggregates melt into spherical liposome shapes. Adding PEG to all three suspensions lowers the suspension viscosity, even though adding PEG increases the viscosity of the saline continuous phase six-fold. This is consistent with a PEG-induced osmotic pressure that dehydrates the multilamellar aggregates, reducing the bilayer spacing and particle volume fraction, which, in turn, reduces the suspension viscosity. Our results parallel the surface rheology of the three surfactants; Survanta has a significantly more viscoelastic interface compared to Infasurf and Curosurf [38-41]. This suggests that the lipid species differences between the three surfactants determine monolayer and bilayer composition and phase behaviour, which in turn, govern the viscoelasticity from suspension to monolayer, and likely also governs the rate of surfactant spreading in the premature lung.

2 Methods

2.1 Materials

Survanta (minced bovine lung or beractant, AbbVie Inc., 25 mg/mL), Infasurf (chloroform/methanol extract of calf lung lavage or calfactant, ONY Inc., 35 mg/mL), and Curosurf (minced porcine lung surfactant or poractant alpha, Chiesi USA Inc., 80 mg/mL) were purchased from the pharmacy at University of Minnesota Boynton Health Service and stored at 4°C until use. Prior to the rheology measurements, the samples were heated in a water bath to the desired temperature. The weight concentration refers to the phospholipid concentration in physiological saline (0.9% w/v) solution but does not account for the small fraction (< 2% by weight) of LS proteins SP-B and SP-C. Polyethylene glycol (PEG) of mean molecular weight of 10 or 20 kDa, was purchased from Sigma Aldrich. 20 kDa PEG was mixed with Curosurf and Infasurf at 5% w/v, while Survanta at 1% w/v (immiscible at higher concentration) for the rheology experiments, while 10 kDA PEG was mixed with all three suspensions at 5% w/v for the SAXS experiments. Previous work showed there were minimal differences in surfactant behavior or depletion forces over this range of PEG molecular weight [42]. The mixtures were vortexed for about 30 seconds until the PEG crystals completely dissolved.

2.2 Cone and plate rheometry

The rheological results presented here are obtained using stress-controlled AR-G2 rheometer from TA Instruments at the University of Minnesota Polymer Characterization Facility. We used a cone and plate fixture with a 40 mm diameter, 2° angle, and 49 µm gap. The plate contains a Peltier plate temperature control system. The cone and plate geometry was chosen to minimize sample volume, although certain samples were also examined using the Couette concentric cylinder (~10 mL) to identify any surface shear effects [43]. Each experiment was performed a minimum of three times and the data reported was the mean ± the standard deviation. The errors were within the size of the symbols used in the figures unless otherwise shown.

Steady shear rheology was used to measure the effective fluid viscosity, η, as a function of shear rate, $\dot{\gamma}$, over the range of $10^{-3} < \dot{\gamma} < \frac{10^3}{s}$ after proper calibration and rotational mapping were performed. In these measurements, the wait time between each subsequent shear rate is 10 seconds. Longer wait times led to evaporation and underfilling at higher temperatures. To reduce evaporation, we used a homemade cover that enclosed both the lateral and the top sides of the cone, with wet paper towels near the sample. This technique provided a humid environment that prevented evaporation for about thirty minutes even at the highest temperatures used. In other experiments, the effective fluid viscosity was measured by a sweep at constant stress to confirm the yield stress of Survanta.

Small amplitude oscillatory shear (SAOS) was used to determine the linear viscoelastic moduli G' and G''. The oscillation amplitudes were adjusted to ensure $G'$and G'' were independent of the applied strain at the frequencies relevant to breathing, i.e., between 0.1-1 Hz, corresponding to 6-60 breaths per minute. The amplitude sweep is shown in the Supplemental Information as Fig. S1.

2.3 Differential Scanning Calorimetry (DSC)

To probe thermodynamic phase changes, differential scanning calorimetry measurements were performed using TA Instruments Q1000 DSC by increasing the temperature from 10°C to 65°C with 2°C/min heating rate after samples were loaded at 23°C and equilibrated at 10°C for 120 s. DSC scans are shown in the Supplementary Materials as Fig. S2.

2.4 Optical microscopy

Optical microscopy analyses of the lamellar structures of the bilayers were performed using an Olympus BX51 Optical Microscope with a Linkam heating stage to probe the structures of the bilayers in

suspension at as a function of temperature. Specimens were examined at their normal hydration or diluted with saline so aggregate flow could be imaged. Bright field images were captured using a QImaging Fast 1394 camera with pixel size of 4.65 µm. Unless otherwise specified, we used 40x magnification objective. The exposure times were manually adjusted depending on the sample contrast.

2.5 Small Angle X-ray Scattering

Small angle x-ray scattering experiments were performed on a custom-built instrument with an 18kW Rigaku rotating anode source (CuK_α., λ = 1.54 Å) and 2-d area detector at room temperature. The instrument is optimized for small angle work (5 - 60 nm), has an Osmic Confocal Maxflux double focusing multilayer mirror, an 11cm Bruker HI-STAR multiwire area detector, and a 1.5m sample to detector distance. The FWHM was less than ~0.005 $Å^{-1}$. In all experiments, the surfactant dispersion in saline were loaded into 1.5 mm borosilicate glass capillaries (Charles Supper, Mass) and flame sealed. Temperature was controlled at 37°C via circulating heated or cooled fluid through an aluminium sample holder block, monitored by a thermistor located adjacent to the capillary [3].

2.6 Freeze-fracture Electron Microscopy

Freeze-fracture samples were prepared by first depositing a film of sample liquid approximately 100 microns thick between two copper planchettes. The samples were frozen by plunging the sample into a liquid propane bath cooled by liquid nitrogen. The frozen sample was transferred under liquid nitrogen to the sample block of a JEM Cryofract freeze-fracture device. The sample was fractured, and the two resulting surfaces were replicated with 1.5 nm platinum deposited at 45˚, followed by 15 nm of carbon deposited normal to the surface. The copper planchettes were dissolved in chromerge (a mixture of chromic acid, sulfuric acid and water), and then the carbon-platinum replicas were washed in water. The replicas were collected on formvar-coated TEM grids (Ted Pella, Redding, California) [44]. A Gatan CCD camera was used to record digital bright field images using a FEI Technai transmission electron microscope at 100 KeV. More details and additional images are available in Braun et al. [3].

2.7 Double-Wall Ring Surface Viscometry

The surface rheology measurement was performed using a TA Instrument double wall ring setup. The lung surfactant suspension was contained in a double-walled circular Teflon trough positioned on top of a Peltier plate, and a platinum-iridium wire ring was attached to a TA Instrument DHR-3 rheometer [45]. The cross section of the ring is square-shaped with a sharp edge to create a planar interface and is ~1 mm in width. After the interface was found, proper calibration was performed before each experiment.

2.8 Centrifugation

To obtain a qualitative estimate of the volume fraction of LS suspension, the suspensions were centrifuged using a benchtop IEC Micromax RF centrifuge at 13600 RPM ($\sim 15000 \times g$) for 60 minutes at 37°C. This was sufficient to cleanly separate the lipid fraction from the solvent fraction and make approximate estimates of the surfactant particle volume fraction. See Supplemental Information Figure S2 for images of the centrifuged samples.

Results and Discussion

3.1 Steady shear rheology

Figure 1 shows the steady shear viscosity of Survanta, Infasurf and Curosurf at 37°C. Banerjee et al. [46] estimated, based on geometrical arguments, that the shear rate experienced by the surfactant flowing through the airway varies from 0.002 s^{-1} to 1.4 s^{-1}. Higher shear rates may be experienced during injection via intratracheal intubation, so our chosen range of measurements covers 10^{-3} s^{-1} to 10^{3} s^{-1}. Surprisingly, the steady shear viscosity of Survanta is roughly two orders of magnitude higher than Infasurf and Curosurf. All three surfactants are strongly shear-thinning; the viscosity of Survanta decreases by more than four orders of magnitude over the tested shear rates, while that of Infasurf and Curosurf decrease by two orders of magnitude. All three suspensions have a Newtonian plateau (arrows in Fig. 1) at shear rates of 10^{-2} s^{-1} and below which can be interpreted as wall slip, which is common in highly concentrated suspensions [1-2]. For shear rates of 1 – 100 s^{-1}, Infasurf and Curosurf are less shear thinning and asymptote to a nearly constant viscosity of $\sim 4\,x\,10^{-3}$ Pa.s similar to the continuous saline suspending fluid of $\sim 10^{-3}$ Pa.s. (Fig. S3 of Supplemental Information) This high shear viscosity regime is similar to

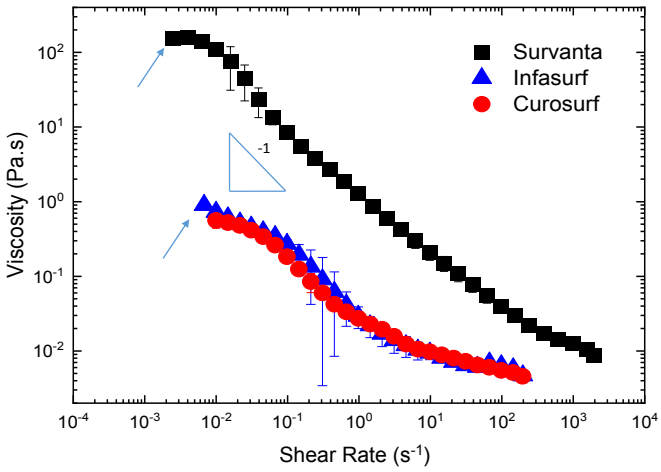

Figure 1. Steady shear viscosity vs shear rate for the clinical surfactants Survanta, Curosurf and Infasurf at 37°C. The three surfactants follow a power-law relationship $\eta = a\dot{\gamma}^m$ with $m \approx -1$ over shear rates from 10^{-2} to 10^{2} s^{-1}. The viscosity of Survanta is two orders of magnitude greater than Curosurf or Infasurf although the lipid mass loading of Survanta is 25 mg/ml, while 35 mg/ml for Infasurf and 80 mg/ml for Curosurf. At the lowest shear rates, a Newtonian plateau (arrows) indicates slip of the concentrated suspension at the walls of the cone and plate [1-2] . Except where noted, the error was smaller than the symbols.

measurements by Thai et al. [22] and Lu et al. [23]. Shear thinning at low shear rates was observed previously in LS dispersions [23, 47], and in other bilayer liposome systems [48-49]. However, most previous work with LS suspensions only considered shear rates greater than ~ 1 s^{-1} at which the surfactant suspensions were close to Newtonian [22-23].

The shear thinning of the three surfactants follows a power-law relationship $\eta = a\dot{\gamma}^m$ over shear rates from 10^{-2} to 10^2 s^{-1} with $-1 \leq m \leq -0.8$ for the three surfactants. Hence, at low shear rates, the shear stress, $\tau = \eta\dot{\gamma}$, is roughly constant, suggesting that these suspensions are sufficiently concentrated to have a yield stress [2]. For practicality, we define yield stress fluids as power law fluids with m values close to -1, instead of fluids that do not flow at all at low shear.

The yield stress in densely packed suspensions must be overcome to initiate flow by deforming the individual particles or by breaking down any long-range structure in the suspension. Figure 2 shows the viscosity as a function of shear stress, $\tau(\dot{\gamma}) = \eta\dot{\gamma}$. All three surfactant suspensions show a nearly constant, Newtonian viscosity below the suspension yield stress: $\tau_{yield} \approx 1$ Pa for Survanta and 0.01 – 0.03 Pa for Curosurf and Infasurf (arrows in Fig. 2). At the yield stress the viscosity drops by orders of magnitude, followed by shear thinning at high shear stresses. Similar results were obtained for Survanta using a sweep at constant stress (open symbols). For both systems, the constant viscosity plateau at low shear stress is consistent with wall slip below the yield stress, which is typical for soft viscoelastic solids [1]. The wall slip likely causes the magnitude of the yield stress to be under-estimated [1]. The two orders of magnitude difference in yield stress carries over from the two orders of magnitude difference in viscosity between Survanta and Infasurf and Curosurf (Fig. 1).

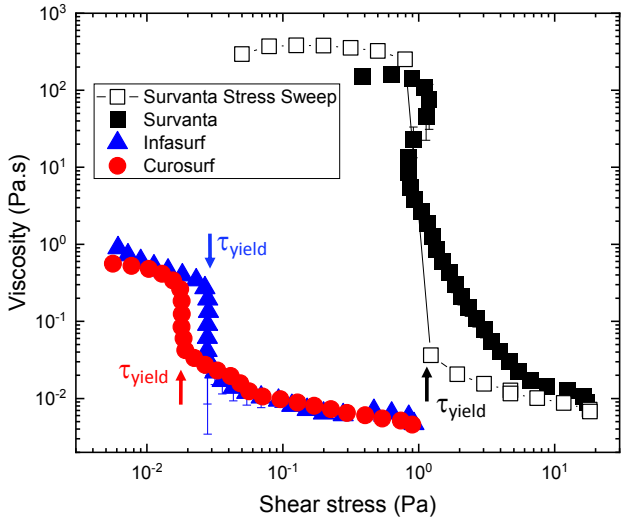

Figure 2. Viscosity vs. shear stress. All three surfactants exhibit the features of yield stress fluids. The Newtonian plateau at shear stresses below the yield stress (arrows) is indicative of wall slip, which is common to concentrated suspensions [1]. The viscosity drops by more than an order of magnitude at the yield stress, and the fluid is weakly shear thinning at higher stresses. The error in measurements is within the size of the symbols used unless noted.

Suspension rheology is typically explained by Eqn. 1, the phenomenological Krieger-Dougherty relationship for concentrated (non-interacting) suspensions as a function of effective particle volume fraction ϕ: [2, 22]

$$\eta = \eta_m\left(1 - \frac{\phi}{\phi_c}\right)^{-[\eta]\phi_c} \qquad (1a)$$

η,η_m,$[\eta]$, and ϕ_c are the suspension viscosity, medium viscosity, intrinsic viscosity (for hard spheres, the value is 2.5), and maximum random packing fraction. For polydisperse hard spheres, $\phi_c \approx 0.7$, which gives the exponent, $[\eta]\phi_c \approx 1.8$. Eqn. 1a predicts that the suspension viscosity is sensitive to small changes in the effective particle volume fraction, ϕ, near the maximum packing fraction, ϕ_c. Hence, if the bilayer aggregate structures of all three lung surfactants were simple hard sphere particles of equal density, Eqn. 1 suggests that Curosurf, with 80 mg/mL lipid loading, should have the highest ϕ , Infasurf, with 35 mg/ml lipid loading should be intermediate, and Survanta, with 25 mg/mL loading, should have the lowest ϕ. Therefore, Eqn. 1 would predict that Curosurf should be the most viscous and Survanta the least viscous which is in direct contrast with the results in Figures 1 and 2.

3.2 Surfactant Aggregate Imaging

Optical and freeze-fracture electron microscopy (Fig. 3) show that the lipid aggregates in Curosurf and Infasurf are multi-layered and spherical. Curosurf (Fig. 3B, E) is more polydisperse with particle sizes ranging from 100 nm to 10 µm [22, 50], while Infasurf (Fig. 3C, F) is more monodisperse with particles around 3 µm. The freeze-fracture

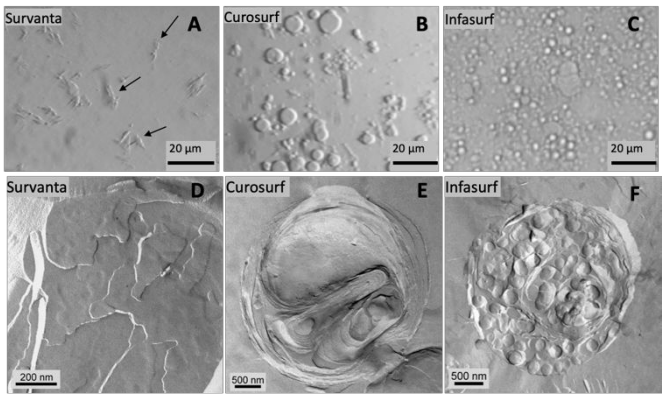

Figure 3. Optical micrographs (top row (**A-C**)) and freeze-fracture transmission electron micrographs (bottom row (**D-F**)) of Survanta, Curosurf and Infasurf showing the differences in bilayer aggregate microstructures. **A)** Survanta consists of 5-20 µm jagged, prolate bilayer aggregates (arrows) with length to width aspect ratios, p ~ 3-6. **D)** The corresponding FFTEM image shows one such flat aggregate surface with multiple bilayer steps. **B)** Curosurf and **C)** Infasurf form spherical multilayered structures of 1 – 10 µm in diameter. However, FFTEM images show **E)** Curosurf has close packed concentric lamellae that are organized like an onion. **F)** Infasurf consists of aggregated unilamellar vesicles and water-filled void spaces. Hence, Curosurf packs more lipid mass within each aggregate than Infasurf so that the volume fractions are similar for these two surfactants. Additional FFTEM images are available in Braun et al. [3].

transmission electron microscopy (FFTEM) images show that the internal organization of the bilayers in the aggregates is quite different (For additional FFTEM images, see Ref. 3)[3]. Curosurf aggregates are organized in onion-like multilayers, with concentric lamellar layers with few internal saline-containing voids (Fig. 3E). Infasurf particles are agglomerations of single bilayer vesicles; the agglomerates also contain multiple water-filled voids (Fig. 3F). Hence, the lipid mass per volume of suspension, c_m and the bilayer aggregate volume fraction, $\phi = \frac{c_m}{\rho}$, depends on ρ, the total lipid mass per total particle volume. This modifies Eqn. 1 to be:

$$\eta = \eta_m \left(1 - \frac{\frac{c_m}{\rho}}{\phi_c}\right)^{-[\eta]\phi_c} \qquad (1b)$$

The FFTEM shows that ρ is quite different between Infasurf and Curosurf. Curosurf packs more lipid into its onion-like multilamellar aggregates than Infasurf with its unilamellar vesicle aggregates, and hence has a higher total lipid mass per particle volume, ρ. Centrifuging the three surfactants shows that the effective surfactant volume fraction $\phi \sim 0.5$ (Fig. S2, Supplemental Materials) for Survanta, Curosurf and Infasurf. Hence, from Eqn. 1b, Curosurf and Infasurf suspensions should have similar viscosities, as we observe.

Survanta aggregates, however, have jagged, prolate shapes, with length to width aspect ratios, p = 3-6 (Fig. 3A, arrows). This is due to the stiffening effect of palmitic acid on the gel phase bilayers of DPPC at and below physiological temperature [14, 19]. PA co-crystallizes with DPPC, which increases the solid to fluid melting temperature to 50-60 °C for the mole ratios of DPPC:PA in Survanta [14, 19] (See Supplementary Information Figure S2). Recent studies by Nakagawa et al. [51-52] showed that mixtures of hexadecanol with saturated phospholipids change the bilayer morphology from spherical vesicles or liposomes to flat, multilamellar sheet-like structures similar to those seen in Survanta. Both palmitic acid and hexadecanol have a small headgroup size that can easily insert in between bulkier headgroups of DPPC, allowing for a stronger van der Waals attraction among the hydrophobic tails, leading to rigid bilayers with greatly increased bending moduli [19, 53-54]. If the resistance to bilayer bending is sufficient, as is also found in the interdigitated phase of saturated phosphatidylcholines, bilayers form stacks of flat sheets rather than closed liposomes [55-56].

The higher aspect ratio p = 3-6 of Survanta aggregates leads to both a higher intrinsic viscosity [η] and a lower critical volume fraction ϕ_c in Eqn. 1 compared to the spherical aggregates in Curosurf or Infasurf. Kuhn and Kuhn [2] proposed for moderate aspect ratios that

$$[\eta] \approx 2.5 + 0.4\,(p-1)^{1.5} \qquad (2)$$

For p = 3, $[\eta] \approx 3.6$. For rod-like structures, the critical packing fraction, ϕ_c of non-Brownian (larger than 1 μm) particles is also a function of the aspect ratio: [57]

$$\phi_c = 0.54 - 0.0125p \qquad (3)$$

which reduces ϕ_c to about 0.5. As a result, there is little change in the exponent in Eqn. 1 as $[\eta]\phi_c \approx 1.8$. However, from centrifuge experiments with Survanta, the particle volume fraction, $\phi \sim 0.5 \sim \phi_c$, or the Survanta volume fraction is close to the critical packing fraction. Hence, the non-spherical shapes of Survanta aggregates lead to the highest viscosity of the three clinical surfactants.

3.3 Thixotropy of Survanta

Dense suspensions are also sensitive to shear history. In thixotropic materials, the viscosity decreases with increasing shear rate, but recovers after a certain rest period. Figure 4 shows the hysteresis of Survanta viscosity for both ascending (filled squares) and descending (open squares) shear rate ramps. The descending shear rate ramp was begun after the sample was allowed two minutes to recover following the ascending ramp. For the first measurement, the shear rate was increased from 0.001 s^{-1} to 1000 s^{-1}, and the descending ramp was performed from 1000 s^{-1} back to 0.01 s^{-1}. As the shear rate was decreased to 0.001 s^{-1} on the descending ramp, the Survanta viscosity decreased by about an order of magnitude relative to the ascending ramp (Compare closed black squares to open black squares).

In measurement 2, the same Survanta sample was subjected to a second shear ramp from 0.01 to 100 s^{-1} following 30 minutes of equilibration time. The ascending branch of the second sweep (filled

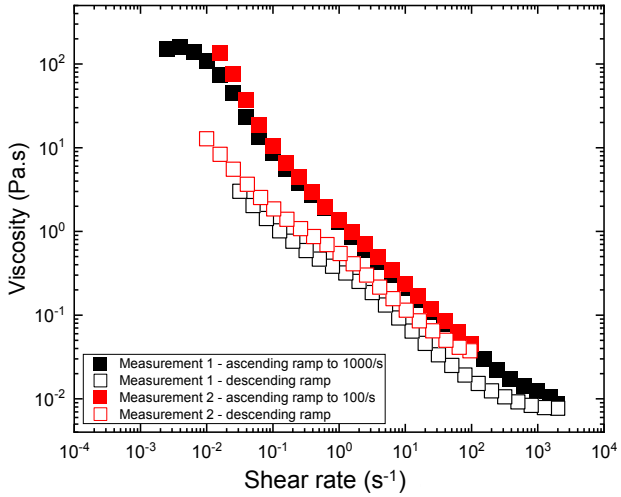

Figure 4. Survanta viscosity shows a significant hysteresis following high shear rates. The descending shear rate ramp (open black squares) was initiated after allowing the suspension to rest for 2 minutes following the ascending ramp to 1000 s^{-1}. The viscosity was reduced by almost an order of magnitude at low shear rates (open black squares). The hysteresis was less pronounced if the ascending ramp was terminated at 100 s^{-1} before initiating the descending ramp after a 2 minute rest. The Survanta structure takes more than 2 minutes to recover its original viscosity. Errors in the measurement are smaller than the size of the symbols used.

red squares) was very similar to the ascending sweep of the first measurement (filled black squares). However, there was less hysteresis on the descending sweep (compare open red squares to open black squares). The difference in the hysteresis suggests that the structure becomes more deformed as the shear rate increases. The two-minute window between ascending and descending ramps was not sufficient for the suspension structure to rebuild. This behavior may be due to some alignment of the prolate Survanta particles at high shear rates that take some time to equilibrate. Thixotropy might also explain discrepancies in viscosity measurements in the literature, especially if high shear rates are examined first by doing the descending shear sweep [22, 50].

3.4 Oscillatory shear rheology

The shear thinning and thixotropic nature of LS suspensions suggests an underlying microstructure that responds to shear. To examine this, oscillatory linear viscoelasticity of the three lung surfactants was probed at 37°C (Figure 5). Amplitude sweep experiments at 0.2 Hz (~ 1 rad-s^{-1}) were done to determine the linear viscoelastic regime for each material, that is how much deformation can be applied before the moduli become dependent on strain (See Supplementary Information Fig. S4). Figure 5 shows that all three demonstrate significant viscoelastic behaviour with the elastic modulus, G', larger than the viscous modulus, G'' at all frequencies tested. When G' is larger than G'', the material can store energy and can return to near its initial configuration like a soft solid [1-2]. Survanta has both G' and G'' higher by ~2 orders of magnitude than Curosurf and Infasurf, meaning that the corresponding complex viscosity, $|\eta^*| = \sqrt{G'^2 + G''^2}/\omega$ of Survanta is also two orders of magnitude larger than that of Curosurf and Infasurf, similar to the trend in steady shear viscosity. Concentrated emulsions, which are somewhat similar in structure to concentrated surfactant suspensions are known to yield

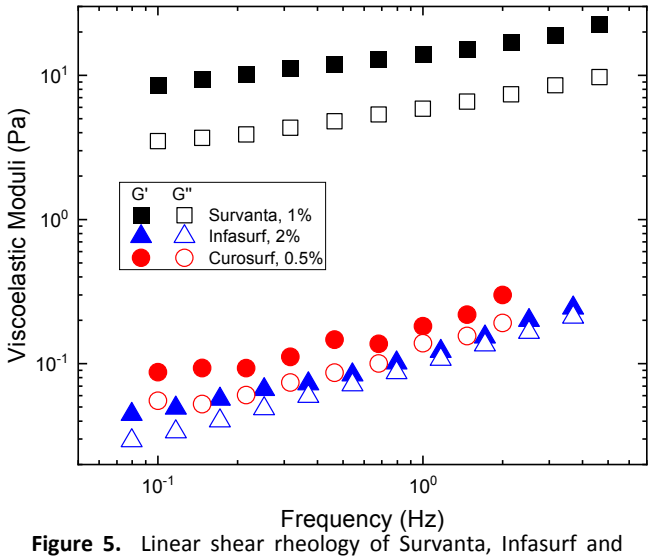

Figure 5. Linear shear rheology of Survanta, Infasurf and Curosurf at oscillatory strains determined to be in the linear regime for each material. All three materials had G'>G" consistent with significant microstructure in the suspension that could store elastic energy over this frequency range. $|\eta*| = \sqrt{(G'^2 + G''^2)}/\omega$ for Survanta is also around two orders of magnitude larger than that of Curosurf or Infasurf, similar to the trend in steady shear viscosity (Fig. 1). Standard deviation of multiple measurements is smaller than the symbols used.

at applied stresses such that $\tau_{yield} \approx {G'}/{10}$ [58-59]. For Survanta $G' \approx 10\ Pa$ and $\tau_{yield} \approx 1\ Pa$, while for Infasurf and Curosurf, $G' \approx 10^{-1}\ Pa$ and $\tau_{yield} \approx .01\ Pa$, surprisingly consistent with this prediction for emulsions [60].

3.5 Temperature effects on Suspension Rheology

Eqns. 1-3 suggest that the prolate structure of Survanta is responsible for the 2 orders of magnitude difference in steady and oscillatory shear viscosity compared to Infasurf and Curosurf. Palmitic acid increases the gel to liquid crystalline transition temperature of DPPC as well as making the bilayers rigid enough that they cannot bend to form spherical structures (Fig. 3A, D). Differential Scanning Calorimetry (DSC) (Fig. S4, Supplemental Information) shows a broad peak centered at 52 °C for Survanta, similar to simple mixtures of DPPC and palmitic acid [14]. Curosurf and Infasurf have broad peaks between 25 and 30 °C [50, 61] showing the lipids are in the fluid state at physiological temperatures. Figure 6A shows the effect of temperature on the Survanta reduced viscosity, η/η_m. The reduced viscosity eliminates the effects of temperature on the solvent (here saline) viscosity, η_m, and highlights the effects on changing the shapes of the Survanta aggregates as manifested in ϕ_c and $[\eta]$ in Eqns. 1-3. Raising the temperature from 5 to 37 °C has a

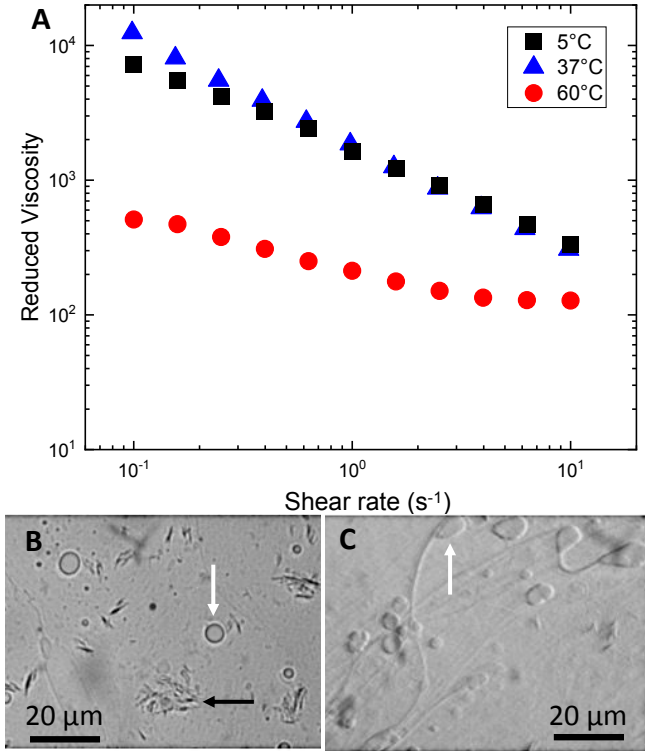

Figure 6. A) Survanta reduced viscosity, η/η_m as a function of shear rate. No difference is observed between 5 and 37 °C, which are below the gel-liquid crystal transition of Survanta. However, the viscosity drops by more than an order of magnitude at 60 °C, above the transition temperature of 52 °C. **B)** Optical microscopy shows that as Survanta is heated above 60 °C, the prolate aggregates (black arrow) melt into spherical shapes (white arrow), similar to those of Curosurf and Infasurf in Fig. 3B, C. **C)** On gentle shear, the Survanta aggregates stuck to the cover slip distort and form extended tubular structures (arrow), similar to bilayer liposomes. This temperature induced change in morphology is responsible for the drop in viscosity of Survanta on heating.

minimal effect on the Survanta reduced viscosity over this range of shear rates. However, at 60 °C, which is above the gel-liquid crystalline transition temperature of Survanta, the reduced viscosity decreases by more than an order of magnitude. Optical microscopy images (Figures 6B, C) show that the prolate Survanta aggregates melt into spherical particles when heated above 60 °C. Under flow, the Survanta aggregates distort into extended shapes, which is common to liposome structures under flow. This transition from prolate to spherical aggregates ($p \rightarrow 1$ in Eqns. 2, 3) reduces the intrinsic viscosity and increases the critical volume faction, ϕ_c, both of which lead to a decrease in the suspension viscosity.

3.6 Polyethylene Glycol Effects on Viscosity

Figure 7 shows that adding 20 kDa molecular weight polyethylene glycol (PEG) reduces the suspension reduced viscosity (η/η_m) for all three clinical surfactants. PEG and other non-adsorbing hydrophilic polymers are added to clinical lung surfactants to promote adsorption to air-water interface in the alveoli that have been contaminated by surface-active serum proteins or lysolipids [15]. Figure 7 shows the reduced viscosity decreased by an order of magnitude or more on addition of PEG compared with neat clinical lung surfactants at 37°C. Adding PEG increases the viscosity of the solvent, η_m, roughly six-fold from 0.7 mPa.s for saline to 4 mPa.s for the PEG-saline at 37°C (Supplemental Information, Fig. S3), even though the suspension viscosity decreased for all three surfactants.

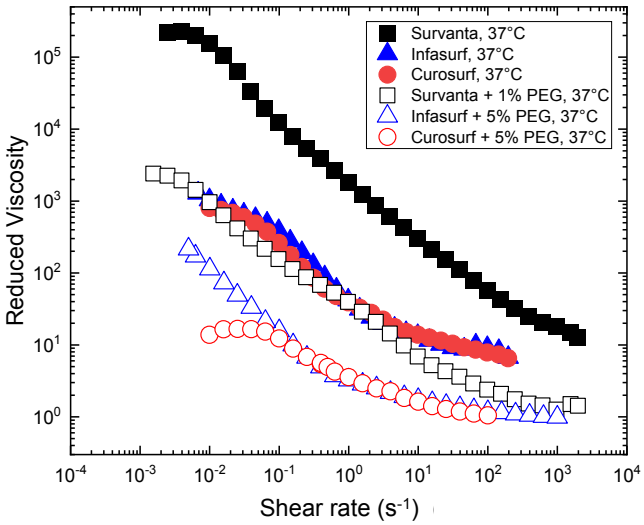

Figure 7. Reduced viscosity, η/η_m as a function of shear rate on addition of polyethylene glycol (PEG) of 20 kDa. The reduced viscosity decreases by an order of magnitude or more on addition of PEG, consistent with a decrease in the particle volume fraction in the suspension caused by the combined effects of osmotic pressure induced dehydration of the surfactant aggregates and a loss of excluded volume due to the depletion attraction.

The added PEG has two effects on the surfactant suspensions, both of which contribute to a decrease in the effective particle volume fraction, ϕ, in Eqn. 1a, b. Macromolecules such as PEG cannot enter the aqueous spaces between bilayers within the surfactant aggregate [3]. This generates a PEG concentration difference between the inside and outside of the aggregate, which in turn, generates an osmotic pressure difference that dehydrates the aggregate, causing a decrease in the bilayer d-spacing, which in turn increases ρ, the total lipid mass per particle volume, and decreases $\phi = c_m/\rho$ at constant c_m.[3]

Small angle X-ray scattering (SAXS) shows that adding PEG dehydrates Survanta and Infasurf aggregates leading to a decrease in the *d-spacing* between the bilayers (Fig. 8). SAXS of both Infasurf (Fig. 8A) and Survanta (Fig. 8B) without PEG showed a number of relatively weak reflections that varied slightly between samples. As both Infasurf and Survanta are multicomponent products derived from organic extraction of bovine lung surfactant, small variations in composition and bilayer spacing are to be expected. The d-spacing

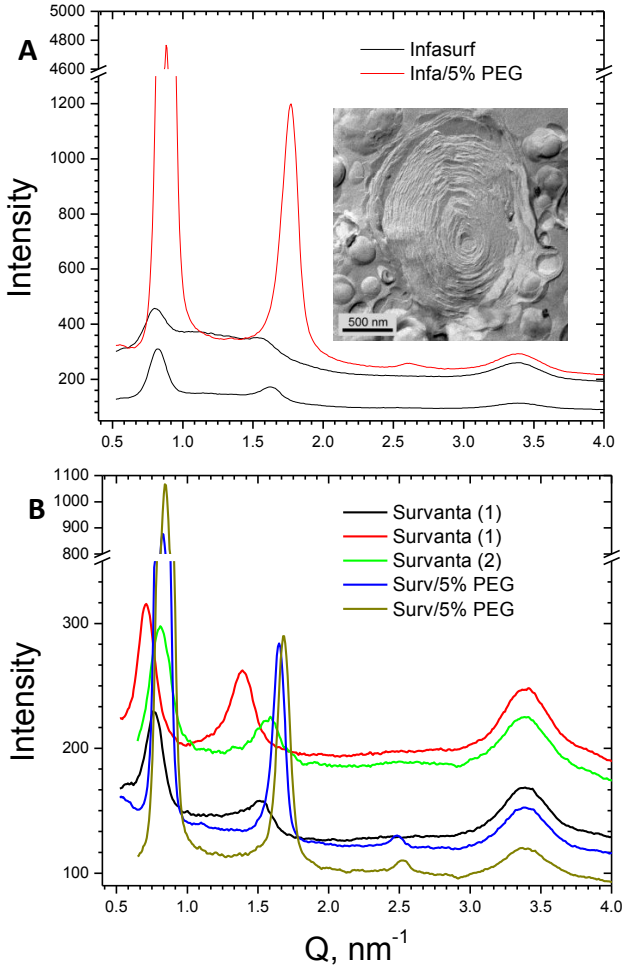

Figure 8. A) Small angle X-ray diffraction patterns of Infasurf and **B)** Survanta with and without added polyethylene glycol polymer (PEG). Without PEG, both Infasurf and Survanta had broad , weak reflections. The d-spacing for Infasurf varied from 7.6 – 7.8 nm and Survanta had 3 repeat spacings of 8.8, 8.3 and 7.8 nm, indicative of lateral phase separation within the bilayers. Adding PEG greatly increased the peak heights for both Infasurf and Survanta, indicating better correlations between the bilayers. The d-spacing for Infasurf decreased to 7.1 nm and 7.6 nm for Survanta. The freeze-fracture inset in **A** shows that the internal organization of Infasurf changed to concentric, tightly packed bilayers with no internal water-filled voids as in Fig. 3F.

for neat Infasurf varied from 7.6 – 7.8 nm, depending on the sample. Neat Survanta had 3 repeat spacings of 8.8, 8.3, and 7.8 nm, indicative of possible lateral phase separation within the bilayers due to segregation of the palmitic acid and DPPC [61]. Similar phase coexistence in bilayers with different d-spacings has been observed in other lung surfactant formulations [62-63].Previous work has shown that neat Curosurf has a bilayer d-spacing of ~ 11 nm [3, 61] that decreases with PEG concentration in a similar fashion. The d-spacings in Fig. 8 are the combined thicknesses of the lipid bilayer and the intercalated saline layer that separates the bilayers in the aggregates.

Adding PEG to Infasurf causes the d-spacing to decrease to 7.1 nm. The osmotic pressure difference imposed by the PEG is balanced against the inter-bilayer repulsion, leading to the decrease in the water thickness separating the lipid bilayers [3]. This dehydration brings the lipid layers closer together and causes much better correlations between the lipid layers. This is indicated by the order of magnitude increases in the peak intensities with added PEG. This enhanced internal ordering of the bilayers is confirmed by the freeze-fracture TEM image of Infasurf with PEG. The freeze-fracture inset in Fig. 8A shows that the internal organization of Infasurf changed to concentric, tightly packed bilayers with no internal water-filled voids as in Fig. 3F [3].

The d-spacing of Survanta decreases to 7.5 - 7.6 nm and the correlations between layers also increase. Dehydrating the surfactant particles leads to a substantial reduction in the effective particle volume fraction, ϕ, and a corresponding decrease in the reduced viscosity according to Eqn. 1. Centrifuging the suspensions also showed this decrease in the particle volume fraction on the addition of PEG compared to the neat suspensions (Fig. S2, Supplemental Information).

The second effect of PEG is to generate weak flocs in the suspension due to the depletion attraction [3, 23]. A mixture of micron sized surfactant particles with nanometer sized macromolecules maximizes its entropy by maximizing the volume accessible per particle [64]. Here, the small particles are the PEG polymers with radius of gyration, R_g (5 - 10 nm), and the large particles are the surfactant aggregates of radius a (typically microns, See Fig. 3A-C). Each large particle immersed in a polymer solution experiences the osmotic pressure induced by the exclusion of PEG from the interior of the surfactant bilayers, acting normal to its surface. For an isolated particle, this pressure is distributed homogeneously over the entire surface, so the net force in any direction is averaged out to zero. However, when two surfactant particles approach each other closer than the effective size of the polymer, $2R_g$, the polymer can no longer fit into the gap between the large spheres. Hence, in the gap between the surfactant particles, the polymer concentration is reduced, resulting in a lower osmotic pressure in the gap. Consequently, the pressure on the surfactant particles due to the polymer osmotic pressure becomes unbalanced, leading to a force that pushes the large particles toward each other, leading to flocculation of the large particles. This is known as the depletion attraction. Moving two surfactant aggregates together decreases the free energy by $3a\phi_p kT/2R_g$, in which ϕ_p is the volume fraction of polymer in the solution. The depletion potential is independent of the chemistry of the surfactant and the polymer, as long as the polymer does not adsorb to surfactant or interface.

The depletion attraction decreases the volume fraction occupied by the surfactant particles and has the largest effect on Survanta at low shear rates. By aggregating, the prolate particles of Survanta take up less excluded volume as rotation is inhibited; the flocculated Survanta particles become more spherical [3]. The depletion attraction provides a more efficient packing in the Survanta suspension, reducing the effective particle volume fraction, ϕ. Previous work has also shown that adding PEG can flocculate and reduce the viscosity of latex suspensions [65]. The difference in reduced viscosity between the neat and PEG Survanta decreases with increasing shear rate as the Survanta flocs are broken up at the higher shear rates.

3.7 Interfacial Shear Viscoelasticity Effects on Suspension Viscosity

As all lung surfactant suspensions are surface-active, lung surfactant will form films at the air-water interface of the cone and plate rheometer. If this surface film is sufficiently elastic, an additional, potentially dominant, contribution to the measured torque may arise, especially as torque scales with distance from the center of the cone [43, 66-68]. In surface-active protein suspensions of albumin or monoclonal antibodies, this interfacial elastic contribution can dominate the bulk contribution in cone and plate measurements and could make the measured suspension viscosity appear as highly viscous and shear-thinning, even if the bulk suspension viscosity was Newtonian and small [43, 66-68]. Distinguishing between the bulk and interfacial contributions to the cone and plate results can be made by measuring the suspension viscosity with a Couette rheometer or other geometry with a much smaller air-water interfacial area per sample volume than the cone and plate geometry [43, 68]. Sharma et al. [43] derived two expressions to describe the effects of interfacial stress on the cone and plate measurements: [43, 68]

$$\eta_{CP}\ (\dot{\gamma}\ ) = \eta_\infty + \frac{3\tau_s}{R\dot{\gamma}} = \eta_\infty + \frac{3\eta_s}{R} \qquad (4)$$

η_{CP} is the suspension viscosity determined with the cone and plate, η_∞ is the suspension viscosity at high $\dot{\gamma}$ (~0.002 Pa.s for the diluted Survanta in Figure 9B), τ_s and η_s are the surface stress and surface viscosity of the Survanta monolayer ($\eta_s\dot{\gamma} = \tau_s$), and R is the radius of the cone and plate. A second model for cone and plate experiments was proposed for surface-active albumin and monoclonal antibody proteins that form elastic, gel-like films with a yield stress ($G_s' > G_s''$ for all frequencies tested in small amplitude oscillatory shear) at interfaces [43, 68]:

$$\eta_{CP}\ (\dot{\gamma}\ ) = \eta_\infty + \frac{3\tau_{s,yield}}{R\dot{\gamma}} \qquad (5)$$

Sharma et al. defined $\tau_{s,yield} = G_s'\,\gamma_{,Yield_S}$ to be the crossover stress at which $G_s' < G_s''$ in a non-linear strain sweep measurement of interfacial moduli at a fixed frequency of $\omega = 1$ rad- s^{-1}[43, 68]. Eqns. 4 and 5 give similar predictions for highly elastic protein films [68]. All

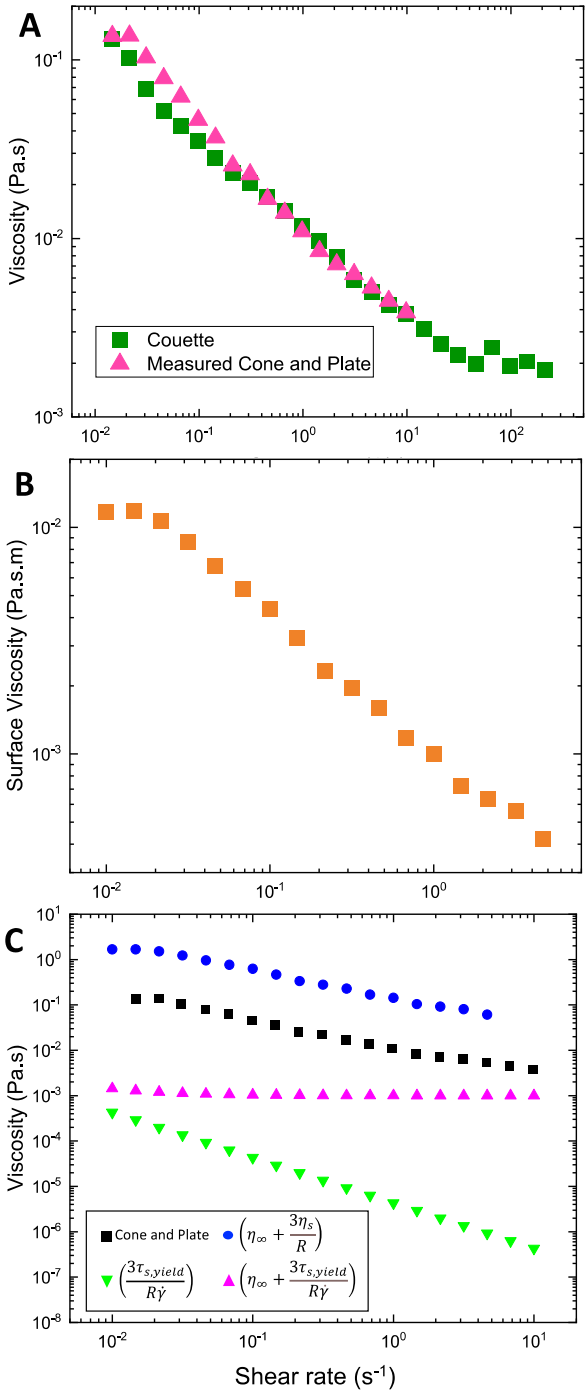

Figure 9. A) Diluted Survanta suspension viscosity measured with a couette viscometer compared to a high interfacial area cone and plate rheometer. No differences were found. **B)** Survanta surface viscosity obtained with a DWR apparatus. The surface viscosity, like the suspension viscosity (Fig. 1) is shear thinning. **C)** Comparison of diluted Survanta suspension viscosity using the cone and plate (black squares) compared to the predicted viscosity using Eqn. 4 (blue circles) and Eqn. 5 (pink triangles). Eqn. 5 suggests a minimal effect of the surface on the cone and plate rheology as observed in **A).**

protein films examined so far were highly elastic, with $G_s' > G_s''$ up to strains of more than 100%, unlike LS monolayers [43, 66-68].

Figure 9A compares the steady shear viscosity measured in a cup and bob Couette geometry for ten-times diluted Survanta with the viscosity measured with the cone and plate. The interfacial viscoelasticity contribution can be identified using rheological probes with different ratios of interfacial area to suspension volume. Unlike the protein suspensions[43, 66-68], the measured viscosities of Survanta are indistinguishable using the two methods. Previous measurements by Lu et al. [23] using a capillary viscometer, for which the interfacial effect is also minimal, gave comparable values to the cone and plate measurements. The similarity in measured values across the different rheological probes with different ratios of interfacial area to suspension volume suggests that interfacial effects do not play a significant role in the measured Survanta bulk viscosity using cone and plate geometry. This is in contrast to protein suspensions whose rheology is dominated by the interfacial elasticity [43, 66-68].

Figure 9B shows the measured steady shear interfacial viscosity of Survanta, η_s, as a function of shear rate using a double wall ring apparatus [45, 68-69]. To form the monolayer on the double wall ring apparatus, Survanta was diluted to 0.8 mg-ml^{-1} in phosphate buffered saline (PBS), and was loaded onto the circular trough and equilibrated for one hour. The equilibrium interfacial tension of Survanta does not change with concentration above a minimum level of ~ 0.1 mg-ml^{-1}; once the interface is saturated, the area per molecule and surface pressure of Survanta is fixed, as is the interfacial viscosity [39, 41, 70]. Like the bulk rheology measured with the cone and plate, the surface viscosity of Survanta was shear thinning with a power law relationship: $\eta_s = a\dot{\gamma}^m$ with $m \sim 0.6$, which is significantly different power law than the measured Survanta bulk viscosity in Fig. 1A that showed $m \sim 1$.

Figure 9C (blue circles) shows the predicted cone and plate viscosity using Eqn. 4 and the surface viscosity measured for the diluted Survanta from Fig. 9B. The black squares in Fig. 9C show that the suspension viscosity of the diluted Survanta measured with the cone and plate is roughly an order of magnitude less than Eqn.4 predicts. As Figure 9A shows, there is a minimal contribution to the suspension viscosity from the interface. This may be because surfactant monolayers are brittle and yield easily. Micro-button surface rheometer measurements showed that the monolayer yield stress for pure dipalmitoylphosphatidylcholine (DPPC is the dominant component in Survanta, Curosurf and Infasurf) is $\tau_{s,yield} \approx 0.01$ μN-m^{-1} [71]. This low yield stress is due to the fracturing of the monolayer at crystalline grain boundaries between ordered DPPC domains [71]. Hermans et al. showed that for Survanta, $G_s' < G_s''$ in linear oscillatory surface viscometry measurements [38], suggesting that $\tau_{s,yield}$ was very small and likely beyond the resolution of the double-wall ring (DWR) surface viscometer. Small strains of 1 - 2% shatter

the DPPC monolayer and $G_s' < G_s''$ and the interface cannot apparently couple to the bulk and contribute to the torque on the cone and plate. Using $\tau_{s,yield}$ in Eqn. 5 shows a negligible surface contribution to the cone and plate rheology (pink triangles), which means that the bulk suspension is responsible for the rheological properties we observe. Curosurf or Infasurf have much lower interfacial shear viscosities than Survanta, which is also likely due to the differences in composition and phase behavior. Protein films act more like a crosslinked gel network and do not yield until large strains of 100% or more are applied [68]. Our results suggest that the interfacial film must be highly elastic and maintain its integrity at large strains to influence the cone and plate measurements.

4. Conclusions

An efficient lung surfactant replacement needs to flow rapidly throughout the airways due to differences in surface tension between the trachea, bronchi and alveoli. During these flows, the shear rate experienced by the surfactant flowing through the airway is estimated to vary from 0.002 s^{-1} to 1.4 s^{-1}. Over these shear rates, Curosurf, Infasurf and Survanta are strongly shear thinning as expected for high volume fraction suspensions; all three surfactants flow like soft solids as shown by $G' > G''$ over a wide range of frequencies in oscillatory viscosity measurements. All three surfactants have an apparent yield stress with Survanta having τ_{yield} ≈ 1 Pa, and Curosurf and Infasurf with τ_{yield} ≈ 0.02 Pa. The two orders of magnitude difference in both shear viscosity and yield stress may be due to the rigid, asymmetric, high aspect ratio particles formed by Survanta (likely due to the high transition temperature of the DPPC-palmitic acid co-crystals) compared to the spherical particles of Curosurf and Infasurf.

The properties of the suspension viscosity were consistent with the phenomenological Krieger-Dougherty relationship (Eqn. 1) for concentrated suspensions of effective volume fraction, ϕ. However, the different surfactant aggregates had quite different internal bilayer organization, which gave quite different relationships between the mass loading given by the manufacturers, and the volume fraction of the particles in the suspension. Both Curosurf and Infasurf formed spherical particles; Curosurf bilayers were organized in concentric layers, like onions, while Infasurf bilayers were organized as agglomerations of unilamellar vesicles. Hence, the density of lipids was lower for Infasurf than Curosurf. This means that the higher mass loading in Curosurf gave a similar volume fraction as the lower mass loading in Infasurf. Survanta consisted of higher aspect ratio (3-6) jagged bilayer crystals, likely due to the addition of palmitic acid to the extracted lipids which stabilizes the crystalline packing in the bilayer. Higher aspect ratio particles decrease the maximum packing fraction [57] in the Krieger-Dougherty model, and for a given particle volume fraction, greatly increase the suspension viscosity, as we observe.

Raising the temperature of the Survanta suspensions above the melting temperature of the bilayer crystals caused a dramatic drop in the suspension viscosity. The high aspect ratio crystals melted into spherical bilayer aggregates similar to Curosurf and Infasurf, which increased the critical packing volume fraction, leading to an order of magnitude decrease in the suspension viscosity.

Adding polyethylene glycol to the suspensions caused significant decreases in the suspension viscosity of all three suspensions, even though adding PEG led to a 6-fold increase in the solvent viscosity. SAXS and freeze-fracture imaging showed the PEG generated osmotic pressure difference between the aggregate interior and exterior, which dehydrated the aggregate bilayers. The bilayer d-spacing decreased for Infasurf and Survanta by ~ 10%; previous results show a similar decrease for Curosurf [3]. PEG also led to depletion-induced flocculation of the three suspensions; this led to an even larger decrease in viscosity as flocculating the high aspect ratio particles provided additional free volume to the suspension. The decrease in suspension volume fractions led to the decrease in suspension viscosity as shown qualitatively by centrifugation, consistent with the Krieger-Dougherty model.

Clinical observations suggest that Survanta takes longer to treat neonatal respiratory distress syndrome following intra-tracheal delivery of the suspension than Curosurf or Infasurf. There is also a higher incidence in deoxygenation following surfactant instillation compared to Infasurf and Curosurf [72-76]. We speculate that these differences are related to our observations that Survanta is a hundred times more viscous with a significantly higher yield stress, which can inhibit spreading by surface tension gradients in the lung. The interfacial viscosity of Survanta is also significantly greater than that of Curosurf or Infasurf, which likely also contributes to slower spreading over the alveolar interfaces. Curosurf delivers the greatest mass of surfactant with the same suspension viscosity as Infasurf.

Author Contributions

C. Ciutara performed the experiments and correlations between theory and experiments. C. Ciutara and J. Zasadzinski wrote the manuscript.

Conflicts of interest

There are no conflicts to declare.

Acknowledgements

This project was supported by National Institutes of Health Grants HL 51177, HL 135065 and NSF Grant CBET 170378. The authors thank H. Warriner for the SAXS measurements, G. Braun for the freeze-fracture imaging and M. Calabrese and C. Macosko for help in interpreting the rheology data.

Notes and references

1. W. B. Russel; M. C. Grant, *Colloid Surf. A-Physicochem. Eng. Asp.* 2000, **161**, 271-282.
2. J. Mewis; N. J. Wagner, *Colloidal Suspension Rheology*. Cambridge University Press: Cambridge, UK, 2012.
3. A. Braun; P. C. Stenger; H. E. Warriner; J. A. Zasadzinski; K. W. Lu; H. W. Taeusch, *Biophys. J.* 2007, **93**, 123-139.
4. S. Schürch; J. Goerke; J. A. Clements, *Proc. Nat. Acad. Sci. USA* 1976, **73**, 4698-4702.
5. S. Schürch; J. Goerke; J. A. Clements, *Proc. Nat. Acad. Sci. USA* 1978, **75**, 3417-3421.
6. S. Schürch; F. H. Y. Green; H. Bachofen, *Biochim. Biophys. Acta* 1998, **1408**, 180-202.
7. J. A. Clements; M. E. Avery, *American Journal of Respiratory and Critical Care Medicine* 1998, **157**, S59-S66.
8. Y. Tanaka; T. Takei; T. Aiba; K. Masuda; A. Kiuchi; T. Fujiwara, *J. Lipid Res.* 1986, **27**, 475-85.
9. W. Bernhard; J. Mottaghian; A. Gebert; G. A. Rau; H. von der Hardt; C. F. Poets, *Am. J. Respir. Crit. Care Med.* 2000, **162**, 1524-1533.
10. W. Bernhard; S. Hoffmann; H. Dombrowsky; G. A. Rau; A. Kamlage; M. Kappler; J. J. Haitsma; J. Freihorst; H. von der Hardt; C. F. Poets, *Am. J. Respir. Cell Mol. Biol.* 2001, **25**, 725-731.
11. R. Veldhuizen; K. Nag; S. Orgeig; F. Possmayer, *Biochimica Et Biophysica Acta-Molecular Basis of Disease* 1998, **1408**, 90-108.
12. D. F. Willson; J. D. Truwit; M. R. Conaway; C. S. Traul; E. E. Egan, *Chest* 2015, **148**, 356-364.
13. J. Bernadino de la Serna; J. Perez-Gil; A. C. Simonsen; L. A. Bagatolli, *J. Biological Chemistry* 2004, **279**, 40715-40722.
14. T. Inoue; S. Yanagihara; Y. Misono; M. Suzuki, *Chemistry and Physics of Lipids* 2001, **109**, 117-133.
15. J. A. Zasadzinski; P. Stenger; I. Shieh; P. Dhar, *Biochemica et Biophysica Acta* 2010, **1798**, 801-828.
16. S. Q. Choi; K. Kim; C. M. Fellows; K. D. Cao; B. H. Lin; K. Y. C. Lee; T. M. Squires; J. A. Zasadzinski, *Langmuir* 2014, **30**, 8829-8838.
17. B. L. Stottrup; S. L. Keller, *Biophys. J.* 2006, **90**, 3176-3183.
18. B. L. Stottrup; J. TigreLazo; V. B. Bagonza; J. C. Kunz; J. A. Zasadzinski, *Langmuir* 2019, **35**, 16053-16061.
19. K. Y. C. Lee; A. Gopal; A. von Nahmen; J. A. Zasadzinski; J. Majewski; G. S. Smith; P. B. Howes; K. Kjaer, *J. Chem. Phys.* 2002, **116**, 774-783.
20. C. Stratton; J. Zasadzinski; D. Elkins, *Anat. Rec.* 1988, **221**, 503-519.
21. J. A. Zasadzinski; C. Stratton; R. Rudolph, *Anat. Rec.* 1988, **221**, 520-532.
22. L. P. A. Thai; F. Mousseau; E. K. Oikonomou; J. F. Berret, *Colloid Surf. B-Biointerfaces* 2019, **178**, 337-345.
23. K. W. Lu; J. Perez-Gil; H. W. Taeusch, *Biochim. Biophys. Acta-Biomembr.* 2009, **1788**, 632-637.
24. A. Z. Stetten; S. V. Iasella; T. E. Corcoran; S. Garoff; T. M. Przybycien; R. D. Tilton, *Curr. Opin. Colloid Interface Sci.* 2018, **36**, 58-69.
25. S. V. Iasella; N. G. Sun; X. Zhang; T. E. Corcoran; S. Garoff; T. M. Przybycien; R. D. Tilton, *J. Colloid Interface Sci.* 2019, **553**, 136-147.
26. K. W. Lu; H. W. Taeusch; B. Robertson; J. Goerke; J. A. Clements, *American Journal of Respiratory and Critical Care Medicine* 2000, **162**, 623-628.
27. K. W. Lu; H. W. Taeusch; B. Robertson; J. Goerke; J. A. Clements, *American Journal of Respiratory and Critical Care Medicine* 2001, **164**, 1531-1536.
28. W. Dehority; K. W. Lu; J. Clements; J. Goerke; J. F. Pittet; L. Allen; H. W. Taeusch, *Pediatric Research* 2005, **58**, 913-918.
29. K. W. Lu; J. Goerke; J. A. Clements; H. W. Taeusch, *Pediatric Research* 2005, **58**, 206-210.
30. K. W. Lu; J. Goerke; J. A. Clements; H. W. Taeusch, *Pediatric Research* 2005, **57**, 237-241.
31. H. W. Taeusch; J. B. de la Serna; J. Perez-Gil; C. Alonso; J. A. Zasadzinski, *Biophys. J.* 2005, **89**, 1769-1779.
32. J. A. Zasadzinski; T. F. Alig; C. Alonso; J. B. de la Serna; J. Perez-Gil; H. W. Taeusch, *Biophys. J.* 2005, **89**, 1621-1629.
33. K. W. Lu; B. Robertson; H. W. Taeusch, *Biology of the Neonate* 2005, **88**, 46-53.
34. J. J. Cummings; B. A. Holm; M. L. Hudak; B. B. Hudak; W. H. Ferguson; E. A. Egan, *Am. Rev. Respir. Dis.* 1992, **145**, 999-1004.
35. J. B. Grotberg, *Annu. Rev. Fluid Mech.* 1994, **26**, 529-571.
36. M. Muradoglu; F. Romano; H. Fujioka; J. B. Grotberg, *J. Fluid Mech.* 2019, **872**, 407-437.
37. M. Filoche; C. F. Tai; J. B. Grotberg, *Proc. Natl. Acad. Sci. U. S. A.* 2015, **112**, 9287-9292.
38. E. Hermans; M. Saad Bhamla; P. Kao; G. G. Fuller; J. Vermant, *Soft matter* 2015, **11**, 8048-57.
39. C. Alonso; A. Waring; J. A. Zasadzinski, *Biophys. J.* 2005, **89**, 266-273.
40. C. Alonso; J. A. Zasadzinski, *Phys. Rev. E* 2004, **69**, 0216021-6.
41. C. Alonso; T. Alig; J. Yoon; F. Bringezu; H. Warriner; J. A. Zasadzinski, *Biophys. J.* 2004, **87**, 4188-4202.
42. P. S. Stenger; S. G. Isbell; J. A. Zasadzinski, *Biochim. Biophys. Acta* 2008, **1778**, 2032-2040.
43. V. Sharma; A. Jaishankar; Y. C. Wang; G. H. McKinley, *Soft Matter* 2011, **7**, 5150-5160.
44. J. A. Zasadzinski; S. M. Bailey, *Journal of Electron Microscopy Technique* 1989, **13**, 309-334.
45. S. Vandebril; A. Franck; G. G. Fuller; P. Moldenaers; J. Vermant, *Rheol. Acta* 2010, **49**, 131-144.
46. R. Banerjee; J. R. Bellare; R. R. Puniyani, *Biochem. Eng. J.* 2001, **7**, 195-200.
47. D. M. King; Z. D. Wang; J. W. Kendig; H. J. Palmer; B. A. Holm; R. H. Notter, *Chemistry and Physics of Lipids* 2001, **112**, 11-19.
48. H. Hoffmann; A. Rauscher; M. Gradzielski; S. F. Schulz, *Langmuir* 1992, **8**, 2140-2146.
49. M. Seth; L. G. Leal, *J. Rheol.* 2014, **58**, 1619-1645.
50. L. P. A. Thai; F. Mousseau; E. Oikonomou; M. Radiom; J. F. Berret, *ACS Nano* 2020, **14**, 466-475.
51. Y. Nakagawa; H. Nakazawa; S. Kato, *J. Colloid Interface Sci.* 2012, **376**, 146-151.
52. Y. Nakagawa; M. Ohta; H. Nakazawa; S. Kato, *Colloid Surf. A-Physicochem. Eng. Asp.* 2014, **443**, 272-279.
53. C. Alonso; F. Bringezu; G. Brezesinski; A. J. Waring; J. A. Zasadzinski, *Langmuir* 2005, **21**, 1028-1035.
54. F. Bringezu; J. Q. Ding; G. Brezesinski; J. A. Zasadzinski, *Langmuir* 2001, **17**, 4641-4648.
55. J. A. Zasadzinski; B. Wong; N. Forbes; G. Braun; G. H. Wu, *Curr. Opin. Colloid Interface Sci.* 2011, **16**, 203-214.
56. B. Wong; C. Boyer; C. Steinbeck; D. Peters; J. Schmidt; R. van Zanten; B. Chmelka; J. A. Zasadzinski, *Adv. Mater.* 2011, **23**, 2320-+.
57. T. Kitano; T. Kataoka; T. Shirota, *Rheol. Acta* 1981, **20**, 207-209.
58. H. M. Princen, *J. Colloid Interface Sci.* 1983, **91**, 160-175.
59. S. M. Fielding; M. E. Cates; P. Sollich, *Soft Matter* 2009, **5**, 2378-2382.
60. S. Y. Choi; S. Steltenkamp; A. J. Pascall; J. A. Zasadzinski; T. M. Squires, *Nature Communications* 2011, **2**, 312.

61. P. L. Oseliero Filho; B. B. Gerbelli; F. Fornasier; A. B. Chaves Filho; M. Y. Yoshinaga; S. Miyamoto; L. Mortara; C. D. Lacerda; I. M. Cuccovia; A. S. Pimentel; C. L. P. Oliveira, *Langmuir* 2020, **36**, 14514-14529.
62. J. B. de la Serna; R. Vargas; V. Picardi; A. Cruz; R. Arranz; J. M. Valpuesta; L. Mateu; J. Perez-Gil, *Faraday Discuss.* 2013, **161**, 535-548.
63. J. R. Fritz; R. W. Loney; S. B. Hall; S. Tristram-Nagle, *Biophys. J.* 2021, **120**, 243-253.
64. S. Asakura; F. Oosawa, *J. Polymer Science* 1958, **33**, 183-192.
65. N. Willenbacher; J. S. Vesaratchanon; O. Thorwarth; E. Bartsch, *Soft Matter* 2011, **7**, 5777-5788.
66. Z. Zhang; S. Barman; G. F. Christopher, *Soft Matter* 2014, **10**, 5965-5973.
67. Z. H. Zhang; S. Barman; G. F. Christopher, *Phys. Rev. E* 2014, **89**, 4.
68. Y. S. Tein; Z. H. Zhang; N. J. Wagner, *Langmuir* 2020, **36**, 7814-7823.
69. T. Verwijlen; P. Moldenaers; J. Vermant, *European Physical Journal-Special Topics* 2013, **222**, 83-97.
70. A. K. Sachan; J. A. Zasadzinski, *Proceedings of the National Academy of Sciences, USA* 2018, **115**, E134-E-143.
71. S. Q. Choi; J. Se Gyu; A. J. Pascall; M. D. Dimitriou; T. Kang; C. J. Hawker; T. M. Squires, *Adv. Mater.* 2011, **23**, 2348-2352.
72. A. M. Fujii; S. M. Patel; R. Allen; G. Doros; C. Y. Guo; S. Testa, *J. Perinatol.* 2010, **30**, 665-670.
73. A. Fujii, *J. Perinatol.* 2010, **30**, 698-698.
74. B. T. Bloom; J. Kattwinkel; R. T. Hall; P. M. Delmore; E. A. Egan; J. R. Trout; M. H. Malloy; D. R. Brown; I. R. Holzman; C. H. Coghill; W. A. Carlo; A. K. Pramanik; M. A. McCaffree; P. L. Toubas; S. Laudert; L. L. Gratny; K. B. Weatherstone; J. H. Seguin; L. D. Willett; G. R. Gutcher; D. H. Mueller; W. H. Topper, *Pediatrics* 1997, **100**, 31-38.
75. C. P. Speer; O. Gefeller; P. Groneck; E. Laufkotter; C. Roll; L. Hanssler; K. Harms; E. Herting; H. Boenisch; J. Windeler; B. Robertson, *Arch. Dis. Child.-Fetal Neonatal Ed.* 1995, **72**, F8-F13.
76. G. F. Fox; R. R. Ci, *Infant* 2005, **1**, 8-12.

